Ghazi et al. Regen Med Ther 2017, 1(1):16-29
Volume 1 | Issue 1

THE SCIENTIFIC PAGES

Regenerative Medicine and Therapeutics

Research Article Open Access

Freeze-Dried Chitosan-PRP Injectable Surgical Implants for Meniscus Repair: Pilot Feasibility Studies in Ovine Models

Ghazi Zadeh L[1], Chevrier A[2], Hurtig MB[3], Farr J[4], Rodeo S[5], Hoemann CD[6] and Buschmann MD[6]*

[1]*Biomedical Engineering Institute, Polytechnique Montreal, Montreal, QC, Canada*

[2]*Chemical Engineering Department, Polytechnique Montreal, Montreal, QC, Canada*

[3]*Department of Clinical Studies, University of Guelph, Guelph, ON, Canada*

[4]*OrthoIndy Knee Care Institute, Cartilage Restoration Center of Indiana, Greenwood, IL, USA*

[5]*Sports Medicine and Shoulder Service, The Hospital for Special Surgery, New York, NY, USA*

[6]*Biomedical Engineering Institute and Chemical Engineering Department, Polytechnique Montreal, Montreal, QC, Canada*

Abstract

Clinical management of meniscus tears often involves partial meniscectomy, which can lead to Osteoarthritis (OA). Meniscus repair augmentation strategies are being developed to compensate for the tissue's limited healing response. The purpose of the study was to assess the feasibility of using implants composed of freeze-dried Chitosan (CS) solubilized in Platelet-Rich Plasma (PRP) to improve meniscus repair in ovine models. Lyophilized formulations containing 1% (w/v) chitosan (degree of deacetylation 82% and number average molar mass 38 kDa), 1% (w/v) trehalose and 42.2 mM calcium chloride were solubilized in autologous PRP and applied to surgically induced meniscus lacerations. In the first study, bilateral tears in 7 ewes were treated by suturing, trephination and injecting either CS-PRP (10 knees) or PRP (4 knees) into the tears. In the second study, unilateral tears in 6 ewes were treated by suturing, trephination and injecting CS-PRP in the tears (2 knees), wrapping the meniscus with a collagen membrane and injecting CS-PRP in the tears and under the wrap (2 knees) or wrapping only (2 knees). CS-PRP implants were partly resident in the tears and trephination channels at 1 day, where they induced cell recruitment from the vascularized periphery of the menisci. Complete repair and seamless repair tissue integration were observed in 1 out of 4 CS-PRP treated defects in the first study after 3 months and in 1 out of 2 CS-PRP treated defects in the second study after 6 weeks, while there was no healing with PRP or wrapping alone. These pilot feasibility studies demonstrated that CS-PRP injectable implants display some potential to improve meniscus repair outcomes in pre-clinical models and could overcome some of the current limitations of meniscus repair by assisting in restoring meniscus structure and function.

Keywords

Meniscus repair, Chitosan, Platelet-rich plasma, Injectable implants, Ovine models

Abbreviations

CS: Chitosan; DDA: Degree of Deacetylation; FBGC: Foreign Body Giant Cell; FD: Freeze-Dried; GAG: Glycosaminoglycan; GP: Glycerol Phosphate; MCL: Medial Collateral Ligament; M_n: Number Average Molar Mass; OA: Osteoarthritis; PRP: Platelet-Rich Plasma; QP: Quantitative Parameter

Introduction

Menisci play a critical role in shock absorption and joint stability [1]. A meniscal tear is one of the most common orthopaedic diagnoses [2] and treatment for meniscal tears account for nearly half of arthroscopic knee procedures performed in the US [3]. Tear characteristics (e.g., tear pattern, length, depth, size, stability of tear, age of tear, chronicity, and reducibility of tear) and patient-related factors (e.g., general health, age, and compliance) all affect the rate of healing and determine the most appropriate treatment for a given patient [4]. Although there has been a recent slight increase in the

number of meniscus repairs performed yearly [5], the percentage of meniscal tears that are considered repairable using existing surgical techniques remains small, and thus the vast majority of tears are excised with partial meniscectomy. Clinical follow-up studies have demonstrated that the risk of developing Osteoarthritis (OA) is increased in patients with untreated meniscal damage or meniscectomized knees [6-8].

The outer 10-30% of the adult meniscus is vascularised [9], giving rise to the clinical labeling of different zones. Vascularity of the meniscus is a prime determinant for the endogenous repair response, and longitudinal tears located in the vascularized red/red portion of the meniscus are considered good candidates for repair. Repair potential is more limited in the inner white/white portion due to a decreased vascular network and a low density of meniscal chondrocytes that fail to migrate to induce a repair response. Several repair augmentation approaches have been proposed in order to stimulate the meniscus healing response to facilitate clinical success [10,11]. These include mechanical stimulation techniques such as trephination, insertion of a duct, abrasion and rasping [12-15], use of patch or scaffold materials [16], and application of blood clots or blood-derived components [17-19]. Although some studies have reported promising findings, there remains a lack of high level evidence to support the use of one augmentation technique over another.

Chitosan is a linear, natural cationic polymer composed of glucosamine and N-acetyl-glucosamine units that has been used for tissue repair and regeneration [20]. Our laboratory has worked extensively with chitosan for cartilage repair applications [21-24]. Chitosan-Glycerol Phosphate (GP) solutions can be mixed with whole blood and applied to microfractured cartilage defects to augment repair [21-24] and is now approved for clinical use to treat cartilage lesions in several countries (BST-CarGel , Smith and Nephew, USA). Some of the mechanisms responsible for this improved outcome have been elucidated in laboratory and animal studies and include an increase in cell recruitment and vascularization, as well as a polarization of the macrophage phenotype towards the alternatively-activated pro-wound healing lineage and stimulated secretion of anabolic wound repair factors [25-27], all of which are also expected to be beneficial in the context of meniscus repair. More recently, we have developed freeze-dried formulations of Chitosan (CS) that can be solubilized in Platelet-Rich Plasma (PRP) to form injectable CS-PRP implants for tissue repair [28]. Lyophilization is expected to provide long-term stability to the product, while PRP constitutes an autologous source of platelet-derived factors and can solubilize lyophilized chitosan for delivery to the wound site to improve repair. In contrast to PRP implants which were rapidly cleared *in vivo* and had little bioactivity, these CS-PRP implants were shown to reside for several weeks and induce vascularization and cell recruitment [28] in a subcutaneous implantation model, both of which are desirable in the context of meniscus repair.

Here we describe two sequential pilot feasibility studies, where we tested the effect of CS-PRP implants in ovine meniscus repair models. In the first study, a bilateral longitudinal surgical laceration model was used to test the hypothesis that meniscus repair is improved by the application of CS-PRP to the tears, but not by application of PRP alone, due to the latter's short-term residency that limits its influence on wound repair, that takes place over several weeks. In the second study, we created a unilateral complex laceration model that was treated with one of 3 approaches; the tears were treated with the CS-PRP implant, or the tears were treated with a wrapping technique using a Geistlich collagen membrane, or the tears were treated with both CS-PRP and the wrapping technique. Our original hypothesis for the second pilot study was that repair outcomes would be improved by using CS-PRP implants in conjunction with the wrapping technique over CS-PRP implants injected in the tear site alone or wrapping alone, due to an increased implant retention and resulting bioactivity. Repair was assessed with histological and electromechanical methods at 3 weeks, 6 weeks and 3 months post-surgery.

Materials and Methods

Preparation of Freeze Dried-Chitosan (FD-CS) formulations

Chitosan (Raw material purchased from Marinard) was processed in-house and the medical-grade polymer was characterized for its Degree of Deacetylation (DDA) and molar mass by NMR spectroscopy and analytical size exclusion chromatography/multi-angle laser light scattering [29,30], respectively. Chitosans with number average molar mass (M_n) of 38 ± 4 kDa and DDA 82 ± 3% were dissolved in 29 mM HCl overnight at room tem-

***Corresponding author:** Michael D Buschmann, Professor, Biomedical Engineering Institute and Chemical Engineering Department, Polytechnique Montreal, PO Box 6079 Succursale Centre-Ville, Montreal, Quebec, H3C 3A7, Canada, Tel: 514-340-4711, Fax: 514-340-2980, E-mail: michael.buschmann@polymtl.ca

Received: June 30, 2017; **Accepted:** September 20, 2017; **Published online:** September 22, 2017

Citation: Ghazi ZL, Chevrier A, Hurtig MB, et al. (2017) Freeze-Dried Chitosan-PRP Injectable Surgical Implants for Meniscus Repair: Pilot Feasibility Studies in Ovine Models. Regen Med Ther 1(1):16-29

perature. Then, a lyoprotectant and a clot activator were added to obtain formulations with final concentrations of 1% (w/v) chitosan, 1% (w/v) trehalose dihydrate and 42.2 mM calcium chloride. This particular formulation was chosen based on our previous work [28] because it met the following performance criteria: 1) Rapid and complete solubilization in PRP; 2) Paste-like properties of the CS-PRP material and fast coagulation; 3) Production of homogenous CS-PRP implants that resist platelet-mediated clot retraction; 4) Significant bioactivity *in vivo* with associated cell recruitment and pro-angiogenic potential. The solutions were sterilized with a 0.22 µm polyvinylidene difluoride filter and dispensed in individual sterile glass vials (1 mL per vial) for freeze-drying. The freeze-drying process was divided into 3 phases: 1) Ramped freezing to -40 °C in 1 hour, isothermal for 2 hours at -40 °C (without applying vacuum); 2) -40 °C for 48 hours, at 100 millitorrs; 3) Ramped heating to 30 °C in 12 hours, isothermal for 6 hours at 30 °C, at 100 millitorrs. Filter-sterile rhodamine-chitosan tracer [31] of M_n 40 kDa was added to the vials that were used for imaging purposes at 1 day post-surgery.

Isolation of Platelet-Rich Plasma (PRP)

On the day of surgery, sodium citrate anti-coagulated whole blood was collected from each sheep and centrifuged with the ACE EZ-PRP system at 160 g for 10 minutes. The supernatant fraction, buffy coat and top ~1

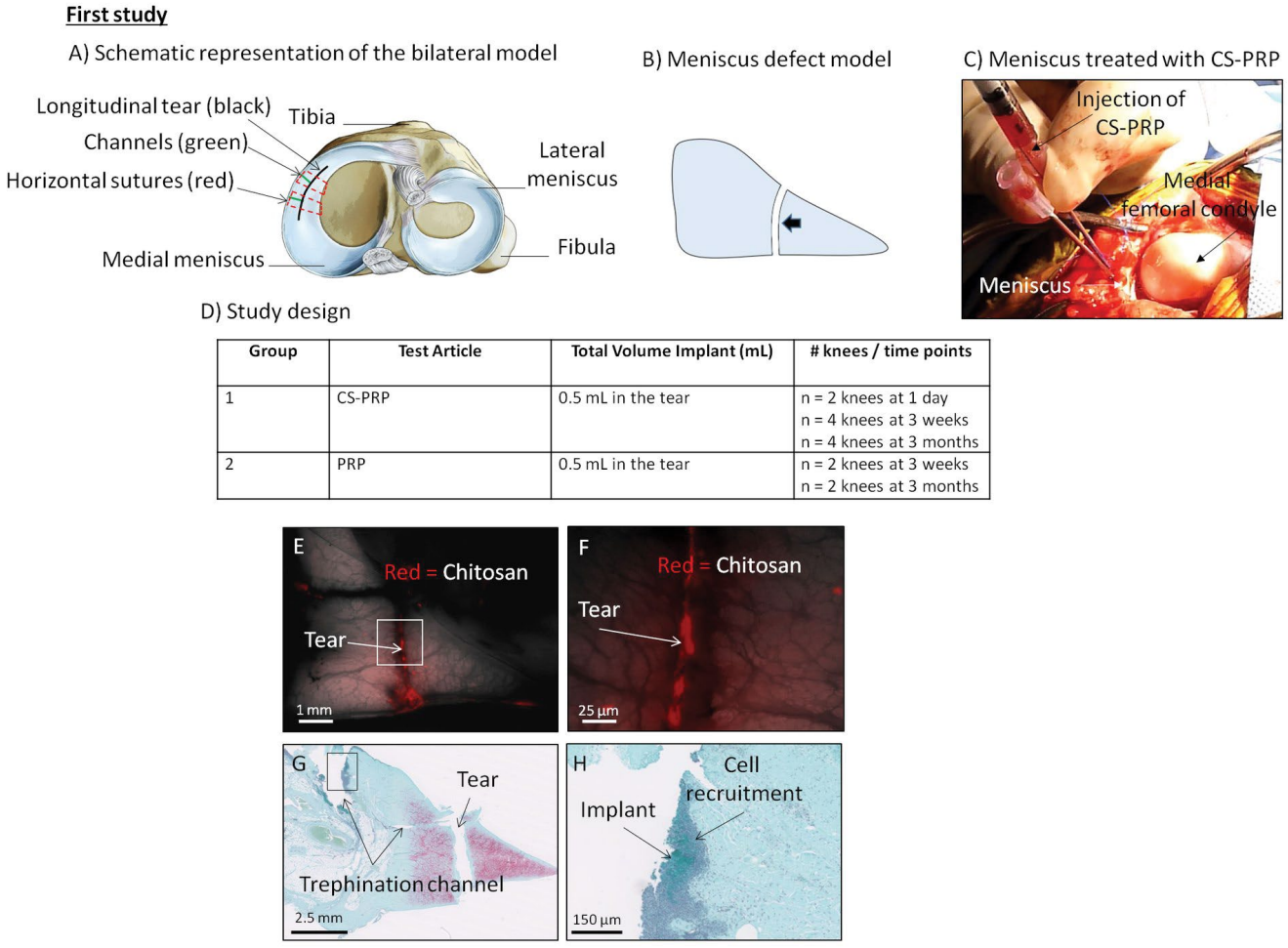

Group	Test Article	Total Volume Implant (mL)	# knees / time points
1	CS-PRP	0.5 mL in the tear	n = 2 knees at 1 day n = 4 knees at 3 weeks n = 4 knees at 3 months
2	PRP	0.5 mL in the tear	n = 2 knees at 3 weeks n = 2 knees at 3 months

Figure 1: A) Schematic representation of the bilateral surgical model. 10 mm long incisions were created bilaterally in the anterior portion of the medial menisci in 7 sheep (black in A). Freeze-dried chitosan formulations were solubilized in autologous PRP and 0.5 mL of chitosan-PRP was injected into the meniscal tear through two trephination channels created with 18-gauge needles (in green in A). The tears were sutured in a horizontal mattress pattern (in red in A); B) Schematic representation of the surgically induced defect model; C) Picture of a meniscus treated with CS-PRP; D) Seven ewes (2-6 years old) were included in the study and treated with either chitosan-PRP only (n = 2 knees at 1 day, n = 4 knees at 3 weeks & 3 months) or PRP only (n = 2 knees at 3 weeks & 3 months); E,F) A rhodamine-chitosan tracer was added to the freeze-dried formulations to allow detection of the implants with epifluorescent microscopy (E,F). The chitosan-PRP implants were partly resident in the tears and trephination channels at 1 day post-surgery (E,F). Safranin O/fast green stained sections showed that chitosan-PRP implants induced cell recruitment from the vascularized periphery of the menisci towards the trephination channels; G,H) The rectangles in panel E,G indicate the regions where the higher magnification images F&H were acquired.

mm of the erythrocyte fraction were moved to another tube and then centrifuged again at 400 g for 10 minutes. Following the second centrifugation step, the supernatant fraction was removed and only the bottom ~1.5 mL fraction of the tube was kept and resuspended to extract Leukocyte-Platelet-Rich Plasma (L-PRP containing leukocytes and a small fraction of erythrocytes). On average, the PRP contained 488 ± 359 × 10 E9/L platelets; 1.6 ± 1.2 × 10 E12/L erythrocytes; and 5.5 ± 3.4 × 10 E9/L leukocytes.

Experimental study design and surgical technique

Institutional animal care committee approvals were obtained for all experiments involving animals, consistent with Canadian Council on Animal Care guidelines. Surgery was conducted under general anesthesia using aseptic technique. Texel-cross ewes aged 2-6 year old with body weights 55-70 kg were used in the first study (n = 7) and in the second study (n = 6).

In the first study (Figure 1), the joints were opened using a ~1.5 cm-long anteromedial arthrotomy to allow access to the anterior portion of the medial meniscus. Bilateral 10 mm long full-thickness longitudinal lacerations were created with scalpel blade and rasped with curved Kelly hemostatic forceps. Two trephination channels were created by inserting 18-gauge needles from the meniscocapsular border to the tears. Freeze-dried chitosan cakes (1 mL) were solubilized with 1 mL autologous PRP and 0.5 mL of CS-PRP was injected into the tears through the two 18-gauge needles (Figure 1). CS-PRP implants have previously been shown to be paste-like and to coagulate within 5 minutes, much more rapidly than recalcified PRP [28]. The tears were secured using two prolene™ sutures in a horizontal mattress pattern 5 minutes after injection. Controls were injected with 0.5 mL of autologous PRP recalcified with 42.2 mM calcium chloride. Acute implant residency was assessed in 1 sheep at 1 day (n = 2 CS-PRP treated knees). Repair was assessed at 3 weeks and at 3 months (n = 4 CS-PRP treated knees and n = 2 PRP treated knees at each time point).

In the second study (Figure 2), the joints were opened using a ~1.5 cm-long anteromedial arthrotomy and greater exposure of the medial compartment was achieved by releasing the Medial Collateral Ligament (MCL) with an attached bone block [32]. A custom-designed 10 mm titanium tool was used to punch out unilateral 10 mm longitudinal lacerations in the anterior portion of the medial meniscus. A sharp scalpel blade was then used to ensure that the tears were full-thickness and to create a 3 mm horizontal pocket from the tears towards the capsular border to introduce a horizontal component and create a complex T-shaped defect [33]. The tears were then rasped and two 20-gauge needles were inserted to create trephination channels from the meniscocapsular

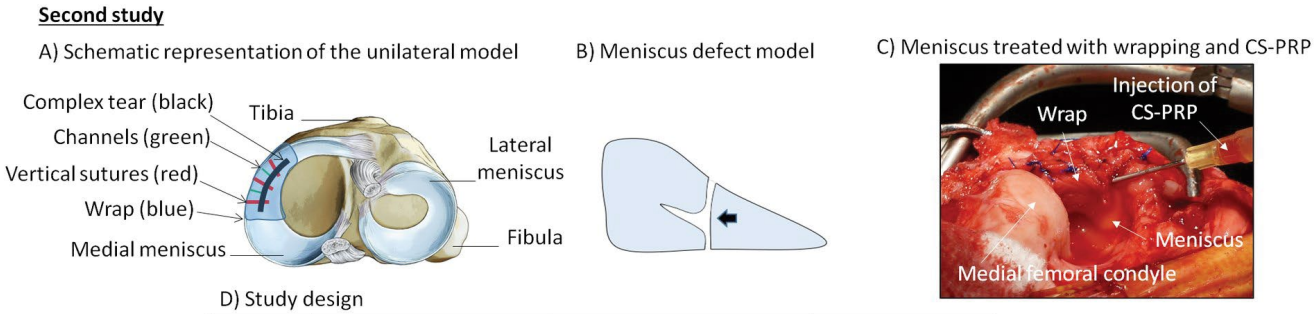

D) Study design

Group	Test Article	Total Volume Implant (mL)	# knees / time points
1	CS-PRP only	0.5 mL in the tear	n = 2 knees at 6 weeks
2	CS-PRP + Wrap	0.5 mL in the tear + 0.5 mL under membrane	n = 2 knees at 6 weeks
3	Wrap only	None	n = 2 knees at 6 weeks

Figure 2: A) Schematic representation of the unilateral surgical model. A bone block with medial collateral ligament attached was detached to increase access to the meniscus. A 10 mm longitudinal tear with a horizontal component was created towards the anterior portion of the medial meniscus (in black A). Two 20-gauge needles were used to create trephination channels from the capsular border of the meniscus to the tear (in green in A). 0.5 mL chitosan-PRP implant was injected into the tear through the trephination channels and the tear was stabilized with three sutures tightened in a vertical pattern (in red A). A piece of collagen membrane (12.5 mm × 25 mm) was wrapped around the meniscus (in blue A) and sutured first at the capsular border, and then with two vertical sutures placed through the meniscal tissue. 0.5 mL chitosan-PRP implant was then injected under the membrane. The contralateral knee was left intact; B) Schematic representation of the surgically induced defect model; C) Picture of a meniscus treated with wrapping +CS-PRP; D) Six ewes (2-6 years old) were included in the study and treated with either chitosan-PRP only (n = 2 knees), chitosan-PRP + wrap (n = 2 knees) or wrap only (n = 2 knees). The contralateral knees were left intact (n = 6 knees).

border to the tear. Freeze-dried chitosan cakes (1 mL) were solubilized with 1 mL autologous PRP and 0.5 mL chitosan-PRP mixture total was injected into the tears through the two 20-gauge needles. Three prolene™ sutures were placed in a vertical pattern to stabilize the meniscus tears and sutures were tightened immediately after implant injection. A 12.5 × 25 mm piece of collagen membrane (Chondro-Gide, Geistlich Pharma) was wrapped around the meniscus and sutured first at the meniscus capsular border, and then further secured by introducing two vertical sutures through the membrane and meniscal tissue. 0.5 mL chitosan-PRP mixture was injected under the membrane (Figure 2) and the bone block was reattached with a screw. The tears were treated by suturing, trephination and either injecting CS-PRP alone (n = 2 knees), injecting CS-PRP and wrapping the meniscus (n = 2 knees) or wrapping alone (n = 2 knees) and healing was assessed at 6 weeks. No post-operative bracing and or knee immobilization was used in both studies.

Evaluation of defect placement

Sheep were sacrificed at 3 weeks, 6 weeks, and 3 months post-surgery using sedation followed by a captive bolt pistol. Photo documentation of the meniscus lesions was performed using a digital camera. Defect placement was assessed with Image J (NIH, USA) by measuring the width between the meniscus outer border and the tear (A) and the total width of the meniscus (B) and calculating the ratio (A/B) × 100%. Values closer to 0% are therefore near the vascularised periphery and values closer to 100% are near the avascular free border.

Electromechanical mapping of articular surfaces

Streaming potentials of cartilage originate from the displacement of positively charged mobile ions in the fluid phase relative to the fixed negatively charged proteoglycans entrapped within the collagen network during a light compression of the cartilage. It has been long established that streaming potentials are particularly sensitive to the integrity of the collagen network of the extracellular matrix and Glycosaminoglycan (GAG) content [34,35]. Several studies have revealed correlations between the electromechanical properties of cartilage and its histological and biochemical properties [36-39]. Electromechanical properties of cartilage are altered by cartilage degeneration and repair [35,38-40]. In the current study, electromechanical properties were mapped manually *ex vivo* across the entire tibial plateau and the distal femurs using the Arthro-BST device (Biomomentum Inc.). This medical device measures streaming potentials generated during a rapid compression of the articular cartilage with an array of microelectrodes lying on a semi-spherical indenter (effective radius of the tip 3.18 mm, 5 microelectrodes/mm^2) [36]. A positioning software with live video feed was used to overlay a 17 × 13 position grid on the articular surfaces to locate measurements and create a uniform mapping. The spherical indenter of the Arthro-BST was manually compressed onto the cartilage surface at each point. The device calculates a Quantitative Parameter (QP, arbitrary units) of cartilage electromechanical activity corresponding to the number of microelectrodes in contact with the cartilage when the sum of their streaming potential reaches 100 mV. A high QP therefore indicates weak electromechanical properties and poor load-bearing capacity and low QP indicates strong electromechanical properties and high load-bearing capacity [36]. Following mapping, osteochondral cores were collected for further processing.

Histoprocessing and microscopic evaluation

Menisci, synovial membrane biopsies and osteochondral cores were fixed in 10% neutral buffered formalin, dehydrated through a graded series of ethanol, cleared in xylene, infiltrated and embedded in paraffin. 5-micrometer-thick sections were collected on slides (Superfrost plus) and stained with iron hematoxylin/safranin-O/fast green (menisci and osteochondral core) or hematoxylin and eosin (synovial membrane biopsies). Stained histological slides were scanned with a Nanozoomer RS (Hamamatsu, Japan) and NDP View (Hamamatsu, Japan) was used to export images for further analysis. Two sections per meniscus were scored by two blinded observers using a scoring system based on Zhang, et al. [41]. Briefly, scores for the character of the predominant tissue, safranin-O staining, surface, integrity, cellularity, repair tissue quality and adjacent tissue quality were summed to obtain the overall tissue quality score (ranging from 0, normal, to 26 for the worst quality). In addition, scores for tissue morphology in the defect, thickness and bonding to host tissue were summed to obtain the repair tissue quality score (ranging from 0, normal, to 7 for the worst quality). Synovial membrane sections were scored as in Little, et al. [42], in which scores for intimal hyperplasia, inflammatory cell infiltration, sub-intimal fibrosis and vascularity are summed to obtain a total score ranging from 0, normal, to 12 for severe abnormalities. Osteochondral sections were scored according to Mankin [43], in which scores for structure, cells, safranin-O staining and tidemark integrity are summed to obtain a final score ranging from 0, normal, to 14 for severe abnormalities.

Data compilation

The data were compiled with SAS Enterprise Guide 7.1 and SAS version 9.4 (SAS Institute Inc, Cary, NC, USA). The data in the text are presented as average ± SD. For each knee, the average of the scores from the 2 readers was calculated and is presented in dot plots.

Table 1: Placement of meniscal defects. Values closer to 0% were near the vascularised periphery and values closer to 100% were near the avascular free border.

First study			Second study		
Sheep (Time)	**Right leg**	**Left leg**	**Sheep (Time)**	**Right leg**	**Left leg**
1 (3w)	PRP 33%	CS-PRP 54%	1 (6w)	Wrap only 55%	Intact N/A
2 (3w)	CS-PRP 56%	PRP 56%	2 (6w)	Intact N/A	44% Wrap only
3 (3w)	CS-PRP** 42%	CS-PRP 40%	3 (6w)	CS-PRP only 51%	Intact N/A
4 (1d)	CS-PRP 44%	CS-PRP 33%	4 (6w)	Intact N/A	CS-PRP only* 45%
5 (3m)	PRP 43%	CS-PRP 58%	5 (6w)	CS-PRP + Wrap 53%	Intact N/A
6 (3m)	CS-PRP 44%	PRP 59%	6 (6w)	Intact N/A	CS-PRP + Wrap** 40%
7 (3m)	PRP 51%	CS-PRP* 45%			

*Defects that were completely healed; **Defects that were partially healed.

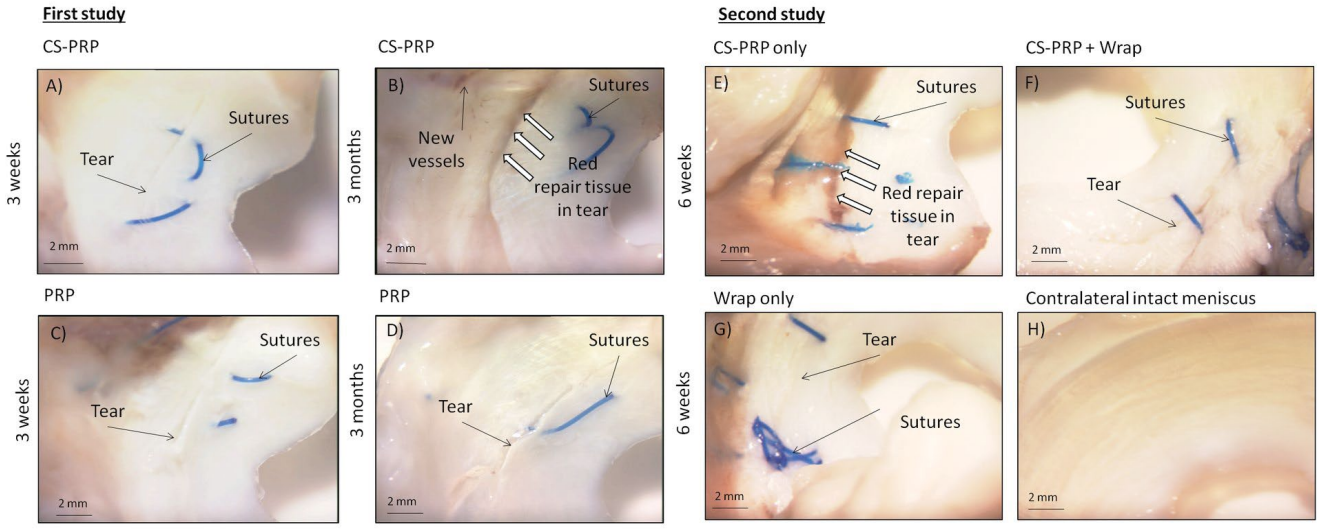

Figure 3: A-G) The tears were macroscopically visible at the time of necropsy 3 weeks, 6 weeks and 3 months after surgery and the edges of the tears were usually well apposed. A reddish repair tissue and signs of neovascularization were visible in two chitosan-PRP treated tears at 6 weeks (E) and at 3 months (B) post-surgery (white arrowheads). Sutures were apparent in all treatment groups. Aside from the surgically-induced tears, no other sign of macroscopic meniscal degeneration was observed.

Results

Meniscus repair is improved in some tears treated with chitosan-PRP implants while no improvement was observed for other treatments.

Surgical lacerations were created on average midway between the capsular borders and the free borders of the menisci (at average 47% ± 9% the length of the meniscus in the first study and 48% ± 6% the length of the meniscus in the second study, Table 1). All the tears were located within the anterior half of each meniscus. CS-PRP implants were easily injected into the tears via trephinations channels where they were shown to be partly resident at 1 day post-surgery (Figure 1E and Figure 1F), and induced cell recruitment from the vascularized peripheral red-red zone towards the trephination channels (Figure 1G and Figure 1H).

All tears were macroscopically visible at the time of necropsy 3 weeks, 6 weeks and 3 months post-surgery and the edges of the tears were usually well apposed with sutures (Figure 3). Aside from the surgically induced tears, no other sign of meniscal degeneration such as fibrillation or structure disruption was observed (Figure 3). Red repair tissue and evidence of neovascularization were visible on the tibial and femoral surfaces of the menisci in two CS-PRP only treated tears at 6 weeks in the second study (1 out of 2 treated defects) and at 3 months in the first study (1 out of 4 treated defects) (Figure 3B and Figure 3E). None of the other menisci displayed macroscopic signs of healing (Figure 3). Extent of healing did not directly correlate with defect location in both studies (Table 1).

A highly cellular repair tissue was seen in 1 out of 4 CS-PRP-treated tear at 3 weeks post-surgery in the first study (Figure 4A and Figure 4B). Partial integration between the repair tissue and the original meniscal tissue was achieved in this treated tear (Figure 4A and Figure 4B). Complete healing with a highly-vascularized repair

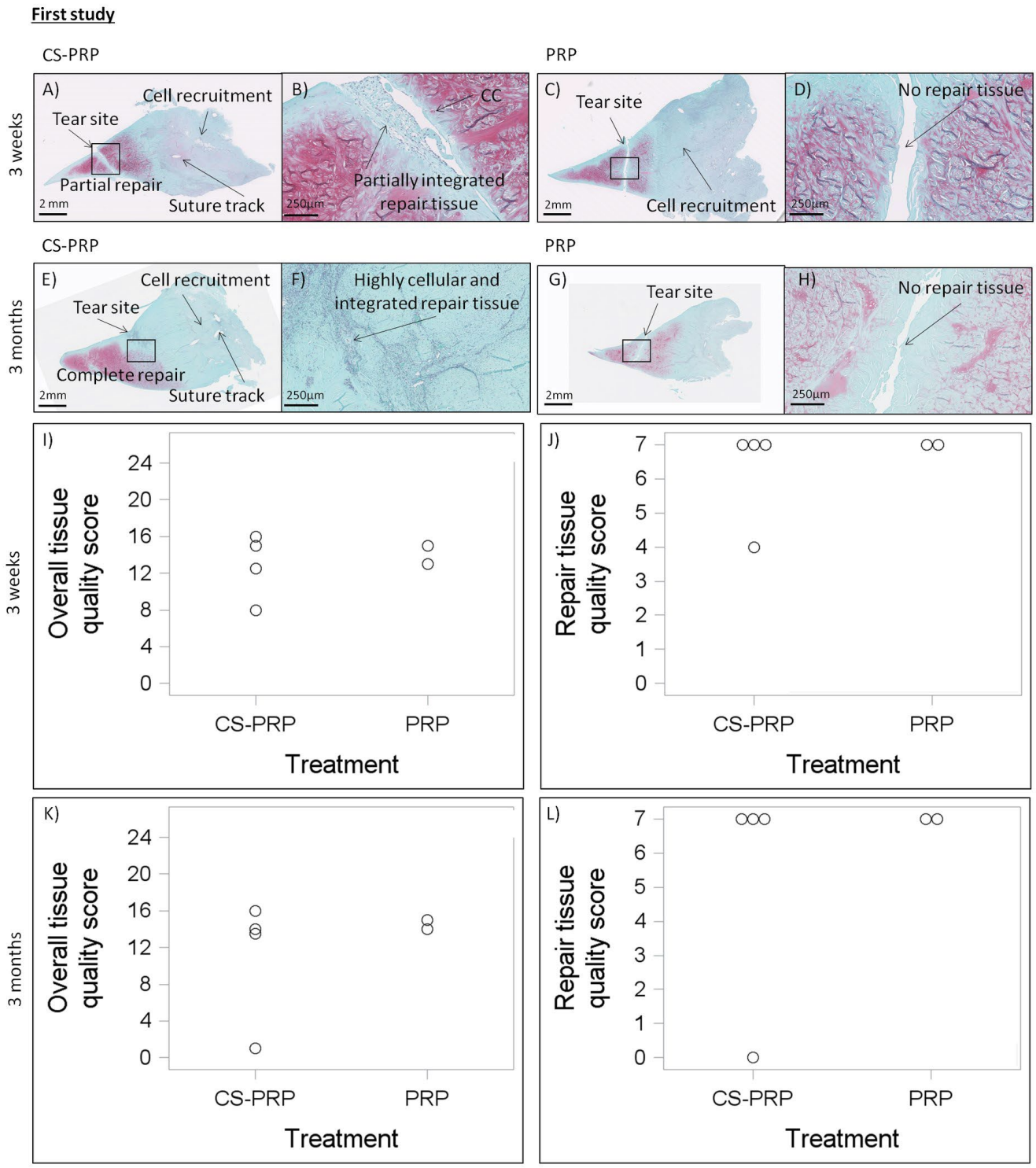

Figure 4: A,B) Histological sections of the repaired tissue stained with safranin O/fast green were used to evaluate tissue repair in the bilateral model. A highly cellular repair tissue was seen in one chitosan-PRP treated tear at 3 weeks post-surgery. Partial integration between the repair tissue and the original meniscal tissue was achieved in this treated tear (B); E,F) Complete healing with a highly vascularized repair tissues and seamless repair tissue integration were seen in one chitosan-PRP treated tear at 3 months; C,D and G,H) There was no repair tissue synthesis in the PRP controls at 3 weeks or at 3 months, and in the other CS-PRP treated tears. The surgical approach induced some fibroplasia in the outer portion of the menisci at 3 weeks and 3 months (A,C,E, and G). Rectangles in panels A,C,E, and G indicate regions where the higher magnification images B,D,F, and H were taken. Histological sections were scored based Zhang, et al. for overall meniscal tissue quality (i, ranging from 0 for the best to 26 for the worst quality) and repair tissue quality (j, ranging from 0 for the best to 7 for the worst quality) and were consistent with the histological observations.

tissue and almost seamless repair tissue integration was seen in 1 out of 4 CS-PRP treated tear at 3 months in the first study (Figure 4E and Figure 4F). No repair tissue synthesis was apparent in any of the PRP control tears at 3 weeks or at 3 months (Figure 4C, Figure 4D, Figure 4G and Figure 4H), or in the other CS-PRP treated tears. Neutrophils were present in the outer vascularized portion of 2 out 4 CS-PRP treated menisci at 3 weeks but were not detected at 3 months, or in any of the PRP treated tears (data not shown). The overall tissue quality score and repair tissue quality score reflected the histological observations with 1 out of 4 treated defects having lower scores indicative of improved quality at 3 weeks (Figure 4I and Figure 4J) and 3 months (Figure 4K and Figure 4L) post-surgery.

Complete healing, seamless integration and a vascularized repair tissue were observed in 1 out of 2 CS-PRP only treated tears after 6 weeks in the second study (Figure 5A, Figure 5B and Figure 5C). Partial repair and integration were observed in 1 out of 2 tears treated with CS-PRP and wrapping at 6 weeks in the second study (Figure 5D, Figure 5E and Figure 5F). In both cases, structural organization was different in matching areas in intact menisci (Figure 5J, Figure 5K and Figure 5L). In contrast, there was no healing in the menisci treated with wrapping alone (Figure 5G, Figure 5H and Figure 5I). Significant cell infiltration at the outer meniscus border and variable Glycosaminoglycan (GAG) depletion was observed in all experimental menisci compared to contralateral intact menisci (Figure 5). Suture tracks were abundant in menisci treated with the wrapping technique (Figure 5D and Figure 5G) with sparse Foreign Body Giant Cells (FBGCs) accumulating near the outer vascularized red-red region (Figure 5F and Figure 5I).

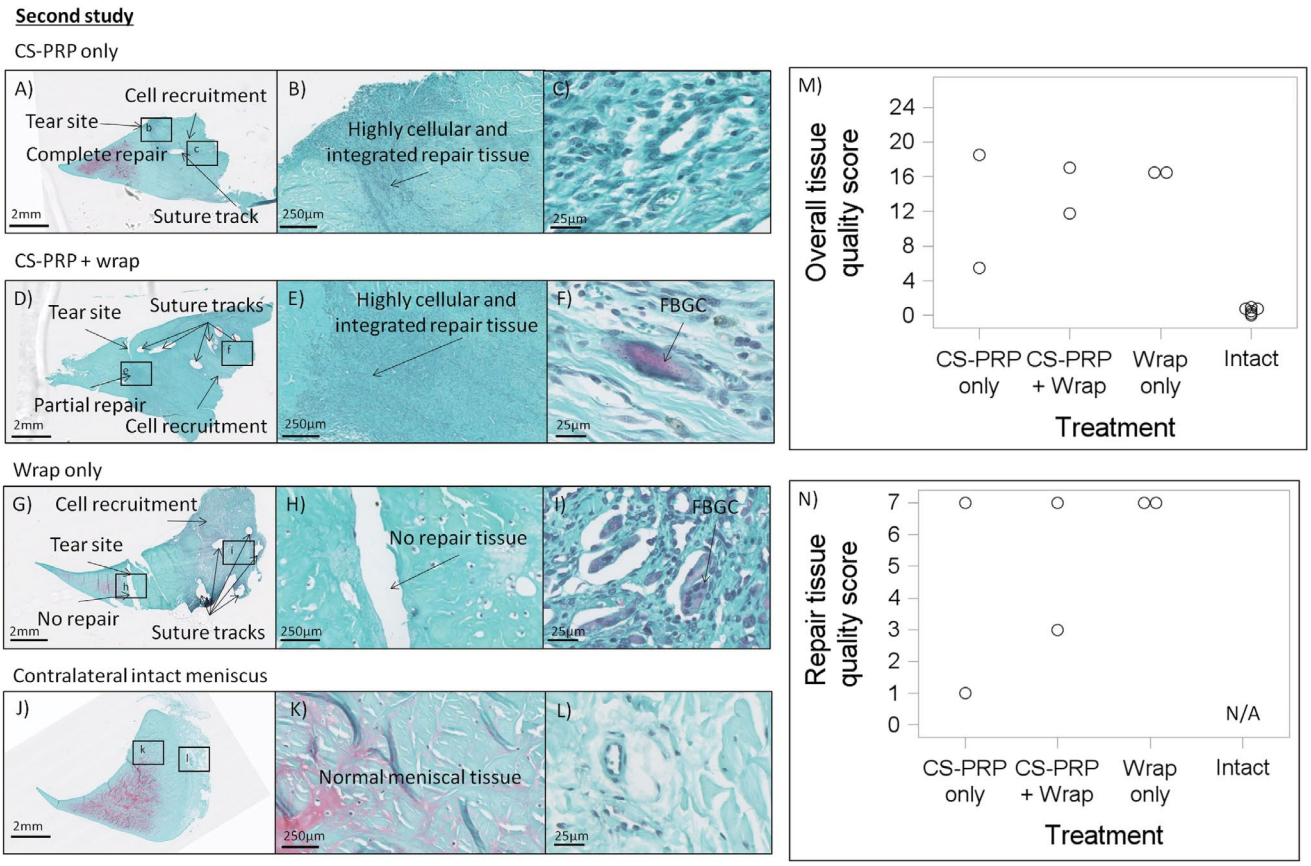

Figure 5: A-C) Histological sections of the repaired tissue stained with safranin O/fast green were used to evaluate tissue repair in the unilateral model; D-F) One tear treated with chitosan-PRP only showed complete repair, while one tear treated with chitosan-PRP with wrapping was partially healed; G-I) There was no repair tissue in the group treated with wrapping only; J-L) In the two cases where repair was observed, the repair tissue was highly cellular, well integrated to the adjacent meniscal tissue, but structurally different than the contralateral intact menisci. Significant cell recruitment into the outer portion of all treated menisci was observed compared to contralateral intact menisci. Suture tracks were frequently observed in menisci treated with the wrapping technique, along with sparse Foreign Body Giant Cells (FBGCs) in the outer vascularized area (D-I). Rectangles in A,D,G and J demonstrate regions where the higher magnification images B,C,E,F,H,I,K and L were acquired. Histological sections were scored based on Zhang, et al. for overall meniscal tissue quality (m, ranging from 0 for the best to 26 for the worst quality) and repair tissue quality (n, ranging from 0 for the best to 7 for the worst quality) and were consistent with the histological observations. N/A: Non applicable.

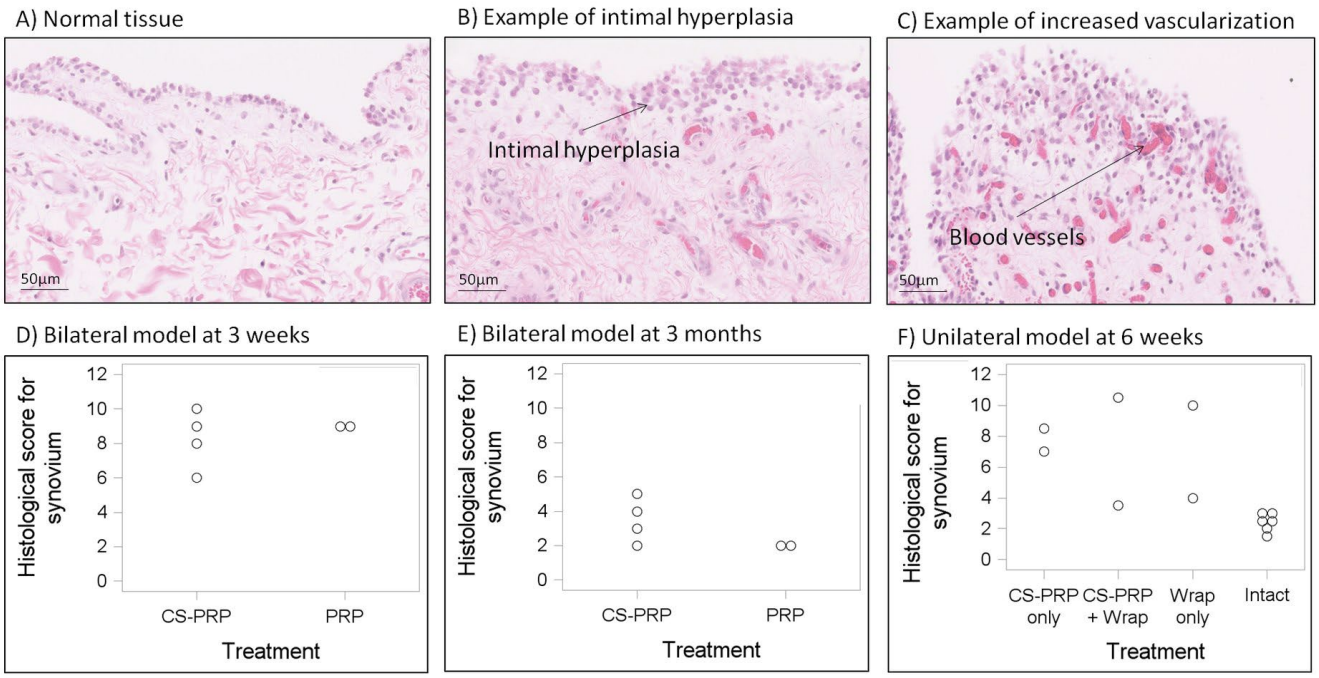

Figure 6: A-C) Hematoxylin and eosin stained sections of synovial membrane. There was a mild to moderate transient synovitis in most treated knees; B) Changes included intimal hyperplasia, inflammatory cell infiltration; C) Some sub-intimal fibrosis, and an increase in vascularization; D-F) Histological sections were scored as in Little, et al. ranging from 0 to 12 for severe abnormalities and scores reflected those observations.

The overall tissue quality score (Figure 5M) and repair tissue quality score (Figure 5N) reflected the histological observations, with one CS-PRP only treated meniscus having the lowest scores (scored 6 and 1 respectively), indicating the highest quality of repair, followed by one meniscus treated with wrapping + CS-PRP (scored 12 and 3 respectively).

Mild changes to other joint tissues were observed and were independent of specific treatments

All animals tolerated the operative approach well and no postoperative complications were seen after the surgery. The sheep had some intermittent lameness and effusion for the first few weeks post-surgery but recovered thereafter. Mild to moderate synovitis was present at 3 weeks and at 6 weeks post-surgery (Figure 6D and Figure 6F), but scores were closer to normal at 3 months (Figure 6E). Changes included intimal hyperplasia, some subintimal fibrosis, and an increase in vascularization (Figure 6A, Figure 6B and Figure 6C), and were not associated with any specific treatment (Figure 6D, Figure 6E and Figure 6F). Mild to moderate histological changes were apparent in the articular cartilage surfaces as shown by safranin-O/fast green stained sections of osteochondral cores collected from the medial femoral condyle and medial tibial plateau (Figure 7). Changes include a loss of glycosaminoglycan and some structural abnormalities (Figure 7B and Figure 7C) and were not specific to any treatment (Figure 7D, Figure 7E and Figure 7F). The average Quantitative Parameter (QP) calculated for the medial femoral condyles and for the medial tibial plateau were similar in all treatment groups at all time points, with values indicative of good load-bearing capacity (Figure 8).

Discussion

The purpose of these pilot studies was to investigate the feasibility of using CS-PRP implants to improve meniscus repair in ovine models. In the first study, we found that CS-PRP implants stimulated repair tissue synthesis in 1 out of 4 treated tears while PRP alone did not, which supports our starting hypothesis. In the second study, in contrast to our original hypothesis, we found that using the meniscus wrapping technique in conjunction with CS-PRP implants did not further improve repair, and that CS-PRP implants alone was sufficient to stimulate repair in 1 out of 2 treated tears.

The bilateral model in the first study (Figure 1) was conceived to control for interindividual variability and minimize the number of required animals. However, we found that it was challenging since it did not permit the sheep to protect their treated knee from weight-bearing post-operatively, which we believe caused some implant loss and led to only partial retention of the CS-PRP implant in the tears (Figure 1) and thus a minority of tears

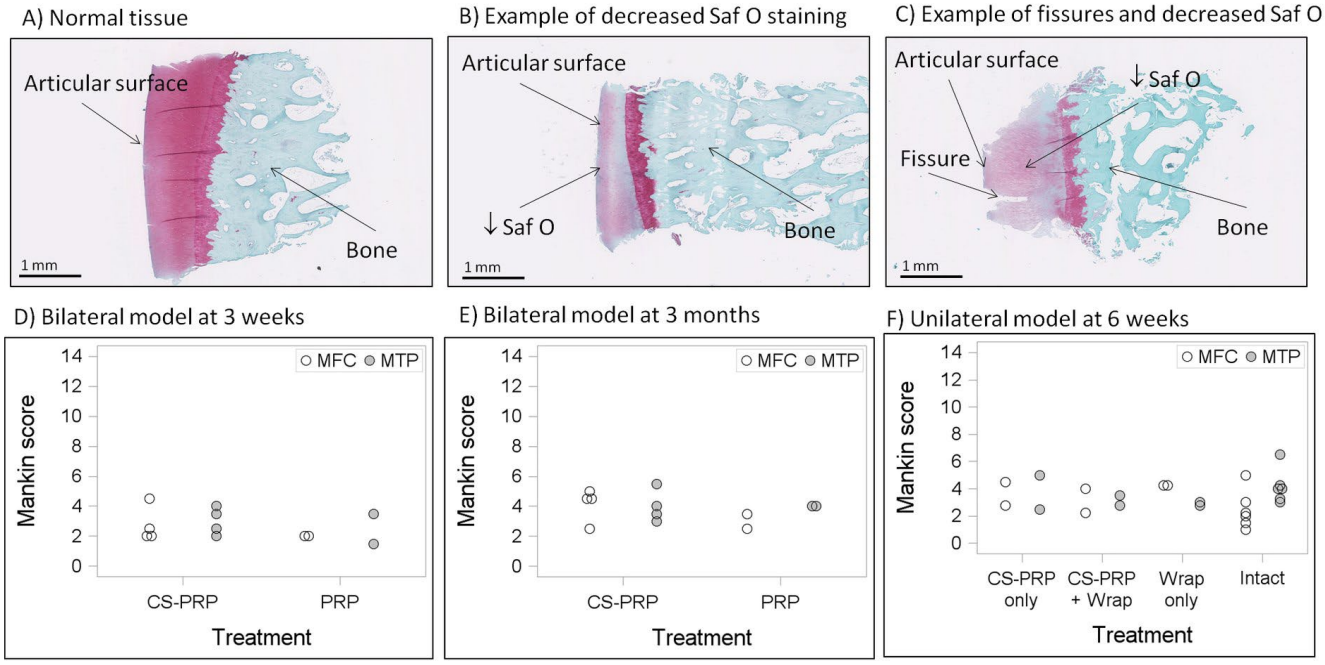

Figure 7: A-C) There were mild to moderate changes to the articular surfaces as shown by safranin O/fast green stained sections of osteochondral cores collected from the medial femoral condyles and from the medial tibial plateau (not shown); B,C) Changes included depletion of glycosaminoglycan and some structural abnormalities. Histological sections were scored according to Mankin (D to F, ranging from 0 to 14 for severe abnormalities) and scores reflected those observations. There was no effect of treatment on the histological scores.

that healed (1 out of 4). The unilateral model in the second study (Figure 2) utilizing a medial collateral bone block approach to the entire meniscus provides increased access to the tear site and allowed us to introduce the meniscus wrapping technique, as well as the T-shaped tears to mimic clinically relevant complex tears. Furthermore, we found that the sheep were protecting the operated knee from weight-bearing post-operatively, which is one potential reason why the success rate was improved to 1 out of 2 treated tears by switching from the bilateral model to the unilateral model. Some form of post-operative immobilization, analogous to the gradual return to weight-bearing protocols used clinically, would be expected to further improve implant retention and the reproducibility of the healing response. Although the tears located closer to the periphery might be expected to heal better, there was no effect of defect placement on healing in our pilot studies (Table 1). Vascular penetration in sheep is less than in humans and is limited to the 11-15% outer region of the meniscus [44], so that all of the tears were in the avascular portion of the meniscus, which may explain why defect placement had no significant effect here.

CS-PRP implants were found to induce cell recruitment as early as one day post-surgery. An immature highly cellular partially integrated tissue filled the tears at 3 weeks (Figure 3 and Figure 4), which was remodeled into a vascularized integrated repair tissue between 6 weeks and 3 months (Figure 3, Figure 4 and Figure 5). The origin of the cells that filled the gap at the defect site was not identified in the current study; however the cells may originate from extrinsic and/or intrinsic sources. The synovial membrane, the peripheral blood supply, and meniscal fibrochondrocytes themselves have all been suggested to be the source of repair in animal studies of meniscus repair [33,45-47]. Meniscal fibrochondrocytes possess the capability to further differentiate towards chondrogenic, adipogenic, and osteogenic lineages [48] and exogenous synovial-derived mesenchymal cells have the capacity of homing and attaching to meniscus tears to mediate reparative process [49]. A combination of healing techniques (e.g. trephination, tear rasping, wrapping and application of CS-PRP) were used in our 2 pilot studies. We used trephination channels to deliver our implants efficiently to the tear site and stimulate healing from the meniscus periphery in a fashion similar to what was previously done in pre-clinical models [50-52], and observed cells migrating towards the channels at 1 day post-surgery, although it is uncertain if those channels remained open and if the cells actually entered the channels to migrate to the tears. Our purpose in rasping the tears was to create a rough surface for the implant to adhere to, but others have suggested that tear rasping can induce cytokine release beneficial to healing [53]. Although this was not done here, synovial rasping

is often performed clinically to stimulate in growth of synovial-derived cells. Further characterization of the type of cells migrating into the defect (for example progenitor cells versus inflammatory cells) and evaluation of cell survival would provide mechanistic information on the repair process, including the origin of the repair cells. Similar to what was observed with CS-GP/blood implants in the context of cartilage repair [26], CS-PRP implants also displayed the potential to induce neovascularization. Based on the histological appearance of our contralateral intact menisci and on previously published data on vascular penetration in sheep meniscus [44], we can state with some confidence that the blood vessels observed in the vicinity of the tears in CS-PRP treated menisci are in fact new blood vessels, and not pre-existing vessels. A better understanding of the vascular response induced by CS-PRP implants would be of high interest for future studies. Our data are also consistent with the notion that remodeling of the meniscus is essential for good tissue integration [54], and it is interesting to note that CS-PRP implants have previously been shown to promote tissue remodeling in the context of cartilage repair [55].

Most available pre-clinical studies have not shown a beneficial effect of applying leukocyte-rich-PRP to meniscal tears [56-59], and clinical data is lacking. We postulate that one reason for the poor performance of PRP is its relatively poor residency *in vivo*. In line with this, we have previously shown that recalcified PRP degrades in a single day when implanted *in vivo*, while CS-PRP implants reside for several weeks and induce cell recruitment and neovascularization [26]. Lyophilized chitosan scaffolds have been proposed as delivery tools for PRP [60-62], and those studies as well as our own preliminary data [63] suggest that chitosan scaffolds can provide sustained release of PRP-derived growth factors, although it is difficult to extrapolate such *in vitro* data regarding platelet derivatives to pre-clinical and clinical settings [64]. Exposure to PDGF-AB has been shown to induce meniscal fibrochondrocytes to proliferate and synthesize new matrix *in vitro* [65]. It therefore becomes logical to suggest that sustained release of platelet-derived growth factors is one mechanism by which CS-PRP implants improved meniscus repair in the current pilot studies. Of note, the single pre-clinical study that reported improved meniscus repair outcomes in the rabbit used a combina-

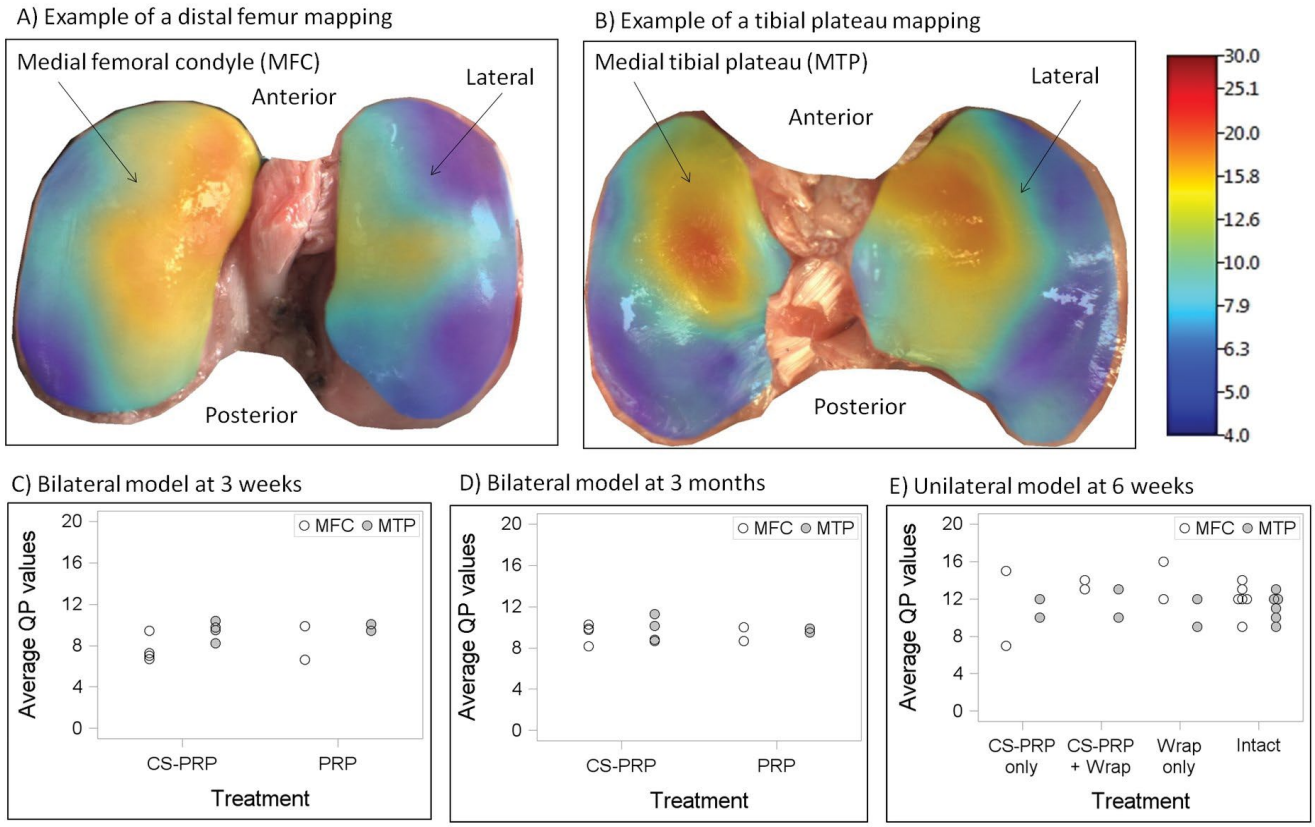

Figure 8: A,B) Electromechanical properties of the tibial plateau and the distal femurs were mapped across the entire articular surfaces using the hand-held Arthro-BST device. Panels a and b are representative examples of mapping of distal femurs (A) and tibial plateau (B) with corresponding QP. A high QP (shown in red) indicates weak electromechanical properties and poor load-bearing capacity and a low QP (in blue) shows strong electro-mechanical properties and high load-bearing capacity. Average QP values for medial femoral condyles and medial tibial plateau are shown in panels C-E and showed that articular surfaces displayed good load-bearing properties. There was no effect of treatment on QP values.

tion gelatin hydrogel for delivery of PRP [66], another biomaterial-PRP combination. N-carboxymethyl chitosan by itself has been shown to modulate the healing sequence in a rabbit model of meniscus repair [67], and we hypothesize that the sustained presence of chitosan at the tear site was another mechanism by which repair was modulated and ultimately improved in the current pilot studies.

Using the wrap in conjunction with CS-PRP implants did not further improve repair and the additional sutures needed to secure the wrap created significant damage to the meniscus (Figure 5). In addition, the wrap appeared to stimulate a foreign body giant cells in wrapped meniscal tissues that was not seen with CS-PRP alone (Figure 5), although foreign body reactions are often observed when very slowly degrading biomaterials are implanted in the body [68]. Although the sheep meniscus is considered an acceptable model [44,69], no animal model is truly like the human, which may account for the poor performance the of the meniscus wrapping technique in the animal model that has uncontrolled post-operative weight bearing compared to humans [16]. The combination of the meniscus wrapping technique with the CS-PRP implants could still prove to be a good option for the clinical treatment of degenerated, complex meniscal tears. CS-PRP implants were well-tolerated and induced only a transient synovitis in the knee (Figure 6). Meniscal damage can easily induce osteoarthritis in the sheep [70], which was not observed here. The histological changes that were observed on the articular surfaces (Figure 7) appear to be normal for sheep of that age and weight [71], and electromechanical mappings (Figure 8) revealed that the articular surfaces had good load-bearing properties [36].

Our study was intended as a pilot feasibility study and had several limitations. The major limitation is the low number of animals used, which precluded statistical analysis, and associated conclusions. Results should therefore be viewed appropriately. Performing these pilot studies allowed us to refine our procedures for design and implantation of the product. We further propose that controlled post-operative weight-bearing would allow for better implant retention and increased reproducibility and efficiency. Clearly, these pilot feasibility studies need to be substantiated in a longer-term follow-up study with a larger number of animals. In light of the results obtained during the second pilot study, groups of n = 25 would be sufficient to allow us to see a statistical difference between the histological quality of the repair tissue elicited by CS-PRP versus wrap treatment (using significance level α of 5% and power 1-β of 80% for calculations). In addition, the mechanical strength of the repair tissue was not assessed, an important factor to prevent recurrent tears. Ideally, functional assessment of the repaired meniscus tissue would be evaluated by biomechanical testing in the future. Another limitation which would be addressed in a subsequent study design would be the addition of sham operated animals and a suture-only group which was absent in the current studies. Finally, sheep are a convenient large-animal model due to availability, geometric similarities between the joints of sheep and humans, ease of handling and housing. Nonetheless, the distribution of forces are quite different in quadruped compared to humans [69].

Meniscus repair remains a significant challenge for orthopaedic surgeons and developing a viable augmentation option is still needed. Freeze-dried chitosan formulations can be rapidly solubilized in autologous PRP to form injectable *in situ* solidifying implants that have tissue regeneration capacity. Even with our pilot studies' limitations, data in this study makes an important advance in showing the importance of using unilateral meniscal repair model, that untreated tears fail to remodel, and that CS-PRP implants displayed some potential to improve repair of meniscal tears, including complex tears. Although further work is required to support these early findings, CS-PRP implants could eventually assist in restoring meniscus structure and function in the future.

Acknowledgements

We thank Geneviève Picard, Gabrielle Deprés-Tremblay, Insaf Hadjab and Sotcheadt Sim for their technical contributions and the funding sources (Ortho Regenerative Technologies Inc, Prima Quebec, Canadian Institutes of Health Research, Canada Foundation for Innovation, Groupe de Recherche en Sciences et Technologies Biomédicales, Natural Sciences and Engineering Research Council of Canada).

References

1. Fithian DC, Kelly MA, Mow VC (1990) Material properties and structure-function relationships in the menisci. Clin Orthop Relat Res 19-31.
2. Clayton RA, Court-Brown CM (2008) The epidemiology of musculoskeletal tendinous and ligamentous injuries. Injury 39: 1338-1344.
3. Kim S, Bosque J, Meehan JP, et al. (2011) Increase in outpatient knee arthroscopy in the united states: a comparison of national surveys of ambulatory surgery, 1996 and 2006. J Bone Joint Surg Am 93: 994-1000.
4. Mordecai SC, Al-Hadithy N, Ware HE, et al. (2014) Treatment of meniscal tears: An evidence based approach. World J Orthop 5: 233-241.
5. Abrams GD, Frank RM, Gupta AK, et al. (2013) Trends in meniscus repair and meniscectomy in the United States, 2005-2011. Am J Sports Med 41: 2333-2339.

6. Englund M, Guermazi A, Roemer FW, et al. (2009) Meniscal tear in knees without surgery and the development of radiographic osteoarthritis among middle-aged and elderly persons the multicenter osteoarthritis study. Arthritis Rheum 60: 831-839.

7. Englund M, Roemer FW, Hayashi D, et al. (2012) Meniscus pathology, osteoarthritis and the treatment controversy. Nat Rev Rheumatol 8: 412-419.

8. Cicuttini FM, Forbes A, Yuanyuan W, et al. (2002) Rate of knee cartilage loss after partial meniscectomy. J Rheumatol 29: 1954-1956.

9. Arnoczky SP, Warren RF (1982) Microvasculature of the human meniscus. Am J Sports Med 10: 90-95.

10. Taylor SA, Rodeo SA (2013) Augmentation techniques for isolated meniscal tears. Curr Rev Musculoskelet Med 6: 95-101.

11. Ghazi zadeh L, Chevrier A, Farr J, et al. (2017) Augmentation techniques for meniscus repair. The Journal of Knee Surgery, In Press.

12. Shelbourne KD, Benner RW, Nixon RA, et al. (2015) Evaluation of peripheral vertical nondegenerative medial meniscus tears treated with trephination alone at the time of anterior cruciate ligament reconstruction. Arthroscopy 31: 2411-2416.

13. Shelbourne KD, Dersam MD (2004) Comparison of partial meniscectomy versus meniscus repair for bucket-handle lateral meniscus tears in anterior cruciate ligament reconstructed knees. Arthroscopy 20: 581-585.

14. Shelbourne KD, Rask BP (2001) The sequelae of salvaged nondegenerative peripheral vertical medial meniscus tears with anterior cruciate ligament reconstruction. Arthroscopy 17: 270-274.

15. Cook JL, Fox DB (2007) A novel bioabsorbable conduit augments healing of avascular meniscal tears in a dog model. Am J Sports Med 35: 1877-1887.

16. Piontek T, Ciemniewska-Gorzela K, Naczk J, et al. (2016) Complex meniscus tears treated with collagen matrix wrapping and bone marrow blood injection: a 2-year clinical follow-up. Cartilage 7: 123-139.

17. Jang SH, Ha JK, Lee DW, et al. (2011) Fibrin clot delivery system for meniscal repair. Knee Surg Relat Res 23: 180-183.

18. Griffin JW, Hadeed MM, Werner BC, et al. (2015) Platelet-rich plasma in meniscal repair: does augmentation improve surgical outcomes? Clin Orthop Relat Res 473: 1665-1672.

19. Pujol N, De Chou ES, Boisrenoult P, et al. (2015) Platelet-rich plasma for open meniscal repair in young patients: Any benefit? Knee Surg Sports Traumatol Arthrosc 23: 51-58.

20. Liu X, Ma L, Mao Z, et al. (2011) Chitosan-based biomaterials for tissue repair and regeneration. Adv Polym Sci 244: 81-128.

21. Hoemann CD, Sun J, McKee MD, et al. (2007) Chitosan-glycerol phosphate/blood implants elicit hyaline cartilage repair integrated with porous subchondral bone in microdrilled rabbit defects. Osteoarthritis Cartiage 15: 78-89.

22. Stanish WD, McCormack R, Forriol F, et al. (2013) Novel scaffold-based BST-CarGel treatment results in superior cartilage repair compared with microfracture in a randomized controlled trial. J Bone Joint Surg Am 95: 1640-1650.

23. Shive MS, Stanish WD, McCormack R, et al. (2015) BST-CarGel® treatment maintains cartilage repair superiority over microfracture at 5 years in a multicenter randomized controlled trial. Cartilage 6: 62-72.

24. Hoemann CD, Hurtig M, Rossomacha E, et al. (2005) Chitosan-glycerol phosphate/blood implants improve hyaline cartilage repair in ovine microfracture defects. J Bone Joint Surg Am 87: 2671-2686.

25. Hoemann CD, Chen G, Marchand C, et al. (2010) Scaffold-guided subchondral bone repair implication of neutrophils and alternatively activated arginase-1+macrophages. Am J Sports Med 38: 1845-1856.

26. Chevrier A, Hoemann CD, Sun J, et al. (2007) Chitosan-glycerol phosphate/blood implants increase cell recruitment, transient vascularization and subchondral bone remodeling in drilled cartilage defects. Osteoarthritis Cartilage 15: 316-327.

27. Fong D, Ariganello MB, Girard-Lauziere J, et al. (2015) Biodegradable chitosan microparticles induce delayed STAT-1 activation and lead to distinct cytokine responses in differentially polarized human macrophages in vitro. Acta Biomater 12: 183-194.

28. Chevrier A, Darras V, Picard G, et al. (2017) Injectable chitosan-platelet-rich plasma (PRP) implants to promote tissue regeneration: In vitro properties, in vivo residence, degradation, cell recruitment and vascularization. Journal of Tissue Engineering and Regenerative Medicine.

29. Lavertu M, Xia Z, Serreqi AN, et al. (2003) A validated 1H NMR method for the determination of the degree of deacetylation of chitosan. J Pharm Biomed Anal 32: 1149-1158.

30. Nguyen S, Winnik FM, Buschmann MD (2009) Improved reproducibility in the determination of the molecular weight of chitosan by analytical size exclusion chromatography. Carbohydrate Polymers 75: 528-533.

31. Ma O, Lavertu M, Sun J, et al. (2008) Precise derivatization of structurally distinct chitosans with rhodamine B isothiocyanate. Carbohydrate Polymers 72: 616-624.

32. Mora G, Alvarez E, Ripalda P, et al. (2003) Articular cartilage degeneration after frozen meniscus and Achilles tendon allograft transplantation: Experimental study in sheep. Arthroscopy 19: 833-841.

33. Ghadially FN, Wedge JH, Lalonde JM (1986) Experimental methods of repairing injured menisci. The Journal of Bone and Joint Surgery 68: 106-110.

34. Sim S, Chevrier A, Garon M, et al. (2014) Non-destructive electromechanical assessment (Arthro-BST) of human articular cartilage correlates with histological scores and biomechanical properties. Osteoarthritis Cartilage 22: 1926-1935.

35. Changoor A, Coutu JP, Garon M, et al. (2011) Streaming potential-based arthroscopic device is sensitive to cartilage changes immediately post-impact in an equine cartilage injury model. J Biomech Eng 133: 061005.

36. Legare A, Garon M, Guardo R, et al. (2002) Detection and analysis of cartilage degeneration by spatially resolved streaming potentials. J Orthop Res 20: 819-826.

37. Sim S, Chevrier A, Garon M, et al. (2017) Electromechanical probe and automated indentation maps are sensitive techniques in assessing early degenerated human articular cartilage. J Orthop Res 35: 858-867.

38. Abedian R, Willbold E, Becher C, et al. (2013) In vitro elec-

tro-mechanical characterization of human knee articular cartilage of different degeneration levels: a comparison with ICRS and Mankin scores. J Biomech 46: 1328-1334.

39. Becher C, Ricklefs M, Willbold E, et al. (2016) Electromechanical assessment of human knee articular cartilage with compression-induced streaming potentials. Cartilage 7: 62-69.

40. Schagemann JC, Rudert N, Taylor ME, et al. (2016) Bilayer implants: electromechanical assessment of regenerated articular cartilage in a sheep model. Cartilage 7: 346-360.

41. Zhang H, Leng P, Zhang J (2009) Enhanced meniscal repair by overexpression of higf-1 in a full-thickness model. Clin Orthop Rel Res 467: 3165-3174.

42. Little CB, Smith MM, Cake MA, et al. (2010) The OARSI histopathology initiative - recommendations for histological assessments of osteoarthritis in sheep and goats. Osteoarthitis Cartilage 18: S80-S92.

43. Mankin HJ, Dorfman H, Lippiello L, et al. (1971) Biochemical and metabolic abnormalities in articular cartilage from osteo-arthritic human hips. II. Correlation of morphology with biochemical and metabolic data. J Bone Joint Surg Am 53: 523-537.

44. Kawai Y, Fukubayashi T, Nishino J (1989) Meniscal suture. An experimental study in the dog. Clin Orthop Relat Res 286-293.

45. Arnoczky SP, Warren RF, Kaplan N (1985) Meniscal remodeling following partial meniscectomy--an experimental study in the dog. Arthroscopy 1: 247-252.

46. Heatley FW (1980) The meniscus--can it be repaired? An experimental investigation in rabbits. J Bone Joint Surg Br 62: 397-402.

47. Mauck RL, Martinez-Diaz GJ, Yuan X, et al. (2007) Regional multilineage differentiation potential of meniscal fibrochondrocytes: implications for meniscus repair. Anat Rec 290: 48-58.

48. Mizuno K, Muneta T, Morito T, et al. (2008) Exogenous synovial stem cells adhere to defect of meniscus and differentiate into cartilage cells. J Med Dent Sci 55: 101-111.

49. Arnoczky SP, Warren RF, Spivak JM (1988) Meniscal repair using an exogenous fibrin clot. An experimental study in dogs. J Bone Joint Surg Am 70: 1209-1217.

50. Zhang ZN, Tu KY, Xu YK, et al. (1988) Treatment of longitudinal injuries in avascular area of meniscus in dogs by trephination. Arthroscopy 4: 151-159.

51. Zhang Z, Arnold JA, Williams T, et al. (1995) Repairs by trephination and suturing of longitudinal injuries in the avascular area of the meniscus in goats. Am J Sports Med 23: 35-41.

52. Ochi M, Uchio Y, Okuda K, et al. (2001) Expression of cytokines after meniscal rasping to promote meniscal healing. Arthroscopy 17: 724-731.

53. Chevrier A, Nelea M, Hurtig MB, et al. (2009) Meniscus structure in human, sheep, and rabbit for animal models of meniscus repair. J Orthop Res 27: 1197-1203.

54. Kambic HE, Futani H, McDevitt CA (2000) Cell, matrix changes and alpha-smooth muscle actin expression in repair of the canine meniscus. Wound Repair Regen 8: 554-561.

55. Dwivedi G, Chevrier A, Hoemann CD, et al. (2016) Freeze dried chitosan/platelet-rich-plasma implants improve marrow stimulated cartilage repair in rabbit chronic defect model. Proceedings of International Cartilage Repair Society, Sorrento, Italy.

56. Zellner J, Hierl K, Mueller M, et al. (2013) Stem cell-based tissue-engineering for treatment of meniscal tears in the avascular zone. J Biomed Mater Res B Appl Biomater 101: 1133-1142.

57. Zellner J, Mueller M, Berner A, et al. (2010) Role of mesenchymal stem cells in tissue engineering of meniscus. J Biomed Mater Res A 94: 1150-1161.

58. Shin KH, Lee H, Kang S, et al. (2015) Effect of leukocyte-rich and platelet-rich plasma on healing of a horizontal medial meniscus tear in a rabbit model. Biomed Res Int 2015: 179756.

59. Lee HR, Shon OJ, Park SI, et al. (2016) Platelet-rich plasma increases the levels of catabolic molecules and cellular dedifferentiation in the meniscus of a rabbit model. Int J Mol Sci 17.

60. Kutlu B, Aydin RST, Akman AC, et al. (2013) Platelet-rich plasma-loaded chitosan scaffolds: Preparation and growth factor release kinetics. J Biomed Mater Res B Appl Biomater 101: 28-35.

61. Shimojo AA, Perez AG, Galdames SE, et al. (2015) Performance of PRP associated with porous chitosan as a composite scaffold for regenerative medicine. ScientificWorldJournal 2015: 396131.

62. Shimojo AA, Perez AG, Galdames SE, et al. (2016) Stabilization of porous chitosan improves the performance of its association with platelet-rich plasma as a composite scaffold. Mater Sci Eng C Mater Biol Appl 60: 538-546.

63. Deprés-Tremblay G, Chevrier A, Tran-Khanh N, et al. (2016) Chitosan-platelet-rich plasma implants for tissue repair - in vitro and in vivo characteristics. 10th World Biomaterials Congress, Montreal, QC, Canada.

64. Borzini P, Mazzucco L (2005) Tissue regeneration and in loco administration of platelet derivatives: clinical outcome, heterogeneous products, and heterogeneity of the effector mechanisms. Transfusion 45: 1759-1767.

65. Tumia NS, Johnstone AJ (2009) Platelet derived growth factor-AB enhances knee meniscal cell activity in vitro. Knee 16: 73-76.

66. Ishida K, Kuroda R, Miwa M, et al. (2007) The regenerative effects of platelet-rich plasma on meniscal cells in vitro and its in vivo application with biodegradable gelatin hydrogel. Tissue Eng 13: 1103-1112.

67. Muzzarelli R, Bicchiega V, Biagini G, et al. (1992) Role of N-Carboxybutyl chitosan in the repair of the meniscus. J Bioact Compat Polym 7: 130-148.

68. Anderson JM, Rodriguez A, Chang DT (2008) Foreign body reaction to biomaterials. Semin Immunol 20: 86-100.

69. Deponti D, Di Giancamillo A, Scotti C, et al. (2015) Animal models for meniscus repair and regeneration. J Tissue Eng Regen Med 9: 512-527.

70. Burger C, Mueller M, Wlodarczyk P, et al. (2007) The sheep as a knee osteoarthritis model: early cartilage changes after meniscus injury and repair. Lab Anim 41: 420-431.

71. Vandeweerd JM, Hontoir F, Kirschvink N, et al. (2013) Prevalence of naturally occurring cartilage defects in the ovine knee. Osteoarthritis Cartilage 21: 1125-1131.